Neuro-Oncology
26(1), 70–84, 2024 | https://doi.org/10.1093/neuonc/noad143 | Advance Access date 8 August 2023

CDK7 and CDK9 inhibition interferes with transcription, translation, and stemness, and induces cytotoxicity in GBM irrespective of temozolomide sensitivity

Isha Bhutada, Fatema Khambati, Shi-Yuan Cheng, Deanna M. Tiek, Derek Duckett, Harshani Lawrence, Michael A. Vogelbaum, Qianxing Mo, Srikumar P. Chellappan, and Jaya Padmanabhan

All author affiliations are listed at the end of the article

*Corresponding Author: Jaya Padmanabhan, Ph.D., Department of Tumor Biology, Moffitt Cancer Center and Research Institute, 12902 Magnolia Drive. (jaya.padmanabhan@moffitt.org).

Abstract

Background. Glioblastoma (GBM) is refractory to current treatment modalities while side effects of treatments result in neurotoxicity and cognitive impairment. Here we test the hypothesis that inhibiting CDK7 or CDK9 would effectively combat GBM with reduced neurotoxicity.

Methods. We examined the effect of a CDK7 inhibitor, THZ1, and multiple CDK9 inhibitors (SNS032, AZD4573, NVP2, and JSH150) on GBM cell lines, patient-derived temozolomide (TMZ)-resistant and responsive primary tumor cells and glioma stem cells (GSCs). Biochemical changes were assessed by western blotting, immunofluorescence, multispectral imaging, and RT-PCR. In vivo, efficacy was assessed in orthotopic and subcutaneous xenograft models.

Results. CDK7 and CDK9 inhibitors suppressed the viability of TMZ-responsive and resistant GBM cells and GSCs at low nanomolar concentrations, with limited cytotoxic effects in vivo. The inhibitors abrogated RNA Pol II and p70S6K phosphorylation and nascent protein synthesis. Furthermore, the self-renewal of GSCs was significantly reduced with a corresponding reduction in Sox2 and Sox9 levels. Analysis of TCGA data showed increased expression of CDK7, CDK9, SOX2, SOX9, and RPS6KB1 in GBM; supporting this, multispectral imaging of a TMA revealed increased levels of CDK9, Sox2, Sox9, phospho-S6, and phospho-p70S6K in GBM compared to normal brains. RNA-Seq results suggested that inhibitors suppressed tumor-promoting genes while inducing tumor-suppressive genes. Furthermore, the studies conducted on subcutaneous and orthotopic GBM tumor xenograft models showed that administration of CDK9 inhibitors markedly suppressed tumor growth in vivo.

Conclusions. Our results suggest that CDK7 and CDK9 targeted therapies may be effective against TMZ-sensitive and resistant GBM.

Key Points

1. CDK7/9 inhibitors suppress the growth and self-renewal of GBM cells and glioma stem cells with minimal cytotoxicity.
2. CDK7/9 inhibition suppresses oncogenic genes and induces tumor suppressors.
3. CDK9 inhibitors abrogate GBM growth in mouse xenograft models.

Glioblastoma (GBM) is the most lethal primary malignant brain tumor in adults, with a median survival of 15-18 months.[1–3] Surgical resection followed by concomitant treatment with radiation and chemotherapy using temozolomide (TMZ)[4] remains the standard of care for GBM. GBM tumors are highly invasive, and complete resection of the tumor-infiltrated areas of the brain is impossible without affecting vital neurological functions. Additionally, GBMs are enriched with

Importance of the Study

We had previously demonstrated that inhibition of CDK7 or CDK9 protects primary neurons against various stress-induced apoptosis. Since cytotoxicity is a major challenge in the current treatments for GBM, we hypothesized that inhibition of CDK7 or CDK9 would selectively eliminate the actively dividing cancer cells and spare the differentiated brain cells from therapy-induced cytotoxicity. Our results support this notion and show that CDK7 and CDK9 inhibitors suppress oncogenes while simultaneously increasing the expression of genes involved in tumor suppression, neuronal activity, differentiation, and growth arrest. Furthermore, these inhibitors significantly constrain the growth of glioma stem cells, which contribute substantially to the GBM heterogeneity, tumor relapse, as well as TMZ-insensitivity. Based on these data and data from the in vivo experiments, we postulate that targeting CDK7 or CDK9 would be beneficial for combating GBM.

glioma stem cells (GSCs), which enable the recurrence of molecularly distinct, aggressive tumors that are resistant to current therapies. The intrinsic tumor cell infiltration and treatment-related cytotoxicity provoke neuronal dysfunction and cognitive impairment in patients, resulting in poor quality of life[5,6]; therefore, effective therapies that are tumor-specific and less neurotoxic are needed to combat GBM.

GBM tumors exhibit dysregulation within multiple regulatory pathways including p53, Rb, and receptor tyrosine kinase-associated signaling cascades.[7–10] Alterations of these pathways allow cells to evade critical tumor suppressive mechanisms such as cell-cycle checkpoints, senescence, and apoptosis, resulting in tumor progression. Despite significant efforts, no novel agents have proven effective against the oncogenic drivers in GBM[11,12]; furthermore, most mono-therapies using targeted inhibitors activate compensatory signaling pathways, resulting in therapy resistance.[13–16] GSCs play critical roles in initiation, invasion, therapy resistance, and recurrence of GBM,[17–20] and are refractory to standard chemotherapy agents; therefore, therapies targeting both the bulk tumor and GSCs are crucial for effective treatment of this disease. Our results predict that inhibitors of CDK7 and/or CDK9 might bring about such an effect and specifically target the actively dividing GBM cells and GSCs while sparing the differentiated brain cells.

CDK7 is a component of the transcription factor TFIIH, which facilitates transcription initiation by phosphorylating Ser-5 in the heptad repeats of the C-terminal domain (CTD) of RNA polymerase II (Pol II).[21] Additionally, CDK7 represents the catalytic subunit of the CDK Activating Kinase complex, which promotes cell-cycle progression. CDK9 is a component of the P-TEFb (CDK9/CyclinT1) complex, which phosphorylates the Pol II CTD at Ser-2 allowing productive elongation and generation of long transcripts from which mRNAs are derived. Previously, we had found that apoptosis in primary neurons is associated with activation of Pol II-dependent transcription and p70S6K-dependent translation.[22] We observed increased expression of CDK7 and CDK9 in the neurons, and the inhibition of transcription using a CDK2/5/7 inhibitor (roscovitine), a CDK4/6/9 inhibitor (flavopiridol), or a RNA Pol II inhibitor (5,6-dichloro-1-β-D ribofuranosyl benzimidazole, DRB), protected the neurons by interfering with both transcription and translation. Based on these observations, we reasoned that inhibition of CDK7 or CDK9 would suppress the growth of actively dividing GBM tumor cells while protecting the post-mitotic neurons. Supporting this notion, it has been shown that the inhibition of CDK7 interferes with super enhancer-associated transcription to suppress GBM growth.[23] We report here that the CDK7 inhibitor THZ1,[24] as well as several CDK9 inhibitors (SNS032,[25] LY2857785,[26] AZD4573,[27,28] NVP2[29] and JSH150[30]) significantly reduce the viability, invasiveness, and self-renewal of GBM cell lines, patient-derived TMZ-responsive and resistant GBM cells, as well as GSCs through inhibition of Pol II and p70S6K. Our data suggest that the CDK7/9 inhibitors could be an attractive option for combating GBM, along with established therapies such as TMZ.

Materials and Methods

Materials

The sources for the cell culture media, CDK7 and CDK9 inhibitors, and the various antibodies are provided in the Supplementary Methods section.

Glioma Patient-Derived Cells, GSCs, and GBM Cell Lines

Previously characterized GSC576 was provided by Dr. Cameron Brennan[31,32]; GBM6 established by Mayo Clinic was from Dr. Derek Duckett.[33] BT89 cells were purchased from ATCC and cultured as suggested by the supplier. Patient-derived TMZ-responsive (GBM42WT) and TMZ-resistant (GBM42R) primary cells were from Dr. Deanna Tiek[34]; the GBM43[35] line established by Mayo Clinic and GSC1478[32] were from Dr. Shi-Yuan Cheng. The GBM cell lines (U87, U251, U251R, T98G and H4) used in this study are described in the Supplementary Methods.

Cell Viability Assay

Viability of indicated cells was measured using either MTT (Methylthiazolyl diphenyl-tetrazolium bromide)[36,37] or CellTiter-Glo assays (see Supplementary Methods).

Nascent Protein Synthesis Assay

Click-iT Plus OPP Protein Synthesis Assay kit with the Alexa Fluor 488 Picolyl Azide from ThermoFisher (Cat # C10456) was used to determine the effect of THZ1 and SNS032 on protein synthesis.

Cell-Cycle Analysis

Propidium iodide staining followed by Flow cytometry was used to analyze the effect of CDK9 inhibitors on cell-cycle progression[36] (see Supplementary Methods).

Western Blot Analysis

Western blotting was conducted as described previously[37]; briefly, GBM cells were treated with the indicated concentrations of the inhibitors; 30-40 μg of proteins were resolved by PAGE and transferred to 0.2 μm nitrocellulose membrane for antibody probing and development using the ECL reagent.

Immunostaining Analysis for BrdU Incorporation

Cells were cultured in poly D-lysine coated 8-chamber slides, treated with the indicated concentrations of SNS032 or THZ1 for 24 hours, incubated with 10 μM BrdU for 4 hours, and immunostained as described previously.[22]

Sphere Formation Assay

To test the effect of CDK inhibitors on the 3D growth and self-renewal, GBM cells were plated in 96-well ultra-low attachment plates at a density of 1000 cells/well in serum-free DMEM/F12 containing EGF, bFGF, and N2 supplements[38] and treated with the indicated inhibitors. The spheres larger than 50 μm were quantified after 8-10 days using an EVOS imaging system.

Colony Formation Assay

Soft agar colony formation assays were performed to determine the effect of drugs on anchorage-independent growth.[37] The colonies were stained with MTT, scanned on an EPSON flatbed scanner, and quantified using *Image J.*

Migration and Invasion Assays

Effect of the drugs on cell migration and invasion was assessed by wound healing and Boyden chamber assays[36] (see Supplementary Methods).

TCGA Data Analysis

The level-3 normalized microarray gene expression data of GBM (n = 502) were obtained from TCGA Cancer Genomics portal (http://firebrowse.org/). The correlations of gene expression among CDK7, CDK9, SOX2, SOX9, and RPS6KB1 (gene for P70S6K) were measured by Pearson correlation coefficient. Relative gene expression across samples is shown on the heatmap based on the z-scores.

Multiplex Imaging of Tumor Microarray

This was conducted using Biosciences OPAL 7-Color Automation IHC kit (Waltham, MA) on the BOND RX autostainer (Leica Biosystems, Vista, CA). After multiplex staining, the slides were imaged with the Vectra3 Automated Quantitative Pathology Imaging System (See Supplementary Methods).

RNA-Seq and RT-PCR Analysis

For RNA-Seq analysis, U251 and U87 cells were treated with 100 nM THZ1 or 500 nM SNS032 for 24 hours, and RNA was isolated using RNeasy mini kit from Qiagen. RNA-seq analysis was conducted by Novogene. For RT-PCR analysis, cDNA synthesized from the RNA was analyzed on a BioRad CFX96 real-time PCR machine using SYBR Green master mix and appropriate primers (See Supplementary Methods).

Orthotopic and Subcutaneous Xenograft Models

All animal experiments were conducted under an IACUC protocol approved by the University of South Florida. For the orthotopic implantation model, 5×10^5 U251-luc cells were implanted into the brains of 8 weeks-old SCID mice. For the subcutaneous xenograft model, 1×10^6 GSC576 cells were suspended in 1:1 Matrigel and implanted on both flanks of nude mice. Once volumes of the tumors reached ~100 mm^3, the mice were randomized into three groups of 8 mice each for treatment with vehicle, SNS032, or AZD4573. Details of the cell implantation, Alzet pump-mediated drug delivery and quantification of the tumors are described in the Supplementary Methods.

Statistical Analysis

All the experiments were conducted at least three independent times. Viability, migration, soft agar colony formation, and self-renewal were conducted in triplicates each time and statistical analysis was performed using *Student's t-test*. Survival analysis was conducted by Kaplan–Meier curve and log-rank (Mantel-Cox) test. Statistical significance was established at $^*P < .05$ ($^{**}P < .01$ and $^{***}P < .001$).

Results

CDK7 and CDK9 Inhibitors Significantly Reduce the Viability of GBM Cells

We first tested the effect of the CDK7 and CDK9 inhibitors, THZ1 and SNS032, on the viability of three different

GBM cell lines by MTT assay. We observed a significant reduction in the viability of H4, U87, and U251 cells after 72 hours of treatment (Figure 1A-C). Both U87 and U251 cells showed sensitivity towards THZ1 and SNS032 at nanomolar concentrations (representative IC_{50} curves for U251 are shown in Figure 1D-E); H4 cells showed an IC_{50} of ~150 nM for THZ1 and ~1.5 μM for SNS032. These data suggest that SNS032 and THZ1 effectively suppress GBM cell viability with high potency.

THZ1 and SNS032 Inhibit Phosphorylation of p70S6K in GBM Cells

Our previous studies demonstrated that the pan-CDK inhibitors flavopiridol and roscovitine interfere with p70S6K activation and translation in primary neurons, while protecting them from apoptosis.[22] Here we tested whether THZ1 or SNS032 affect p70S6K in GBM cells. As shown in Figure 1F-1G, U87 and H4 cells treated with

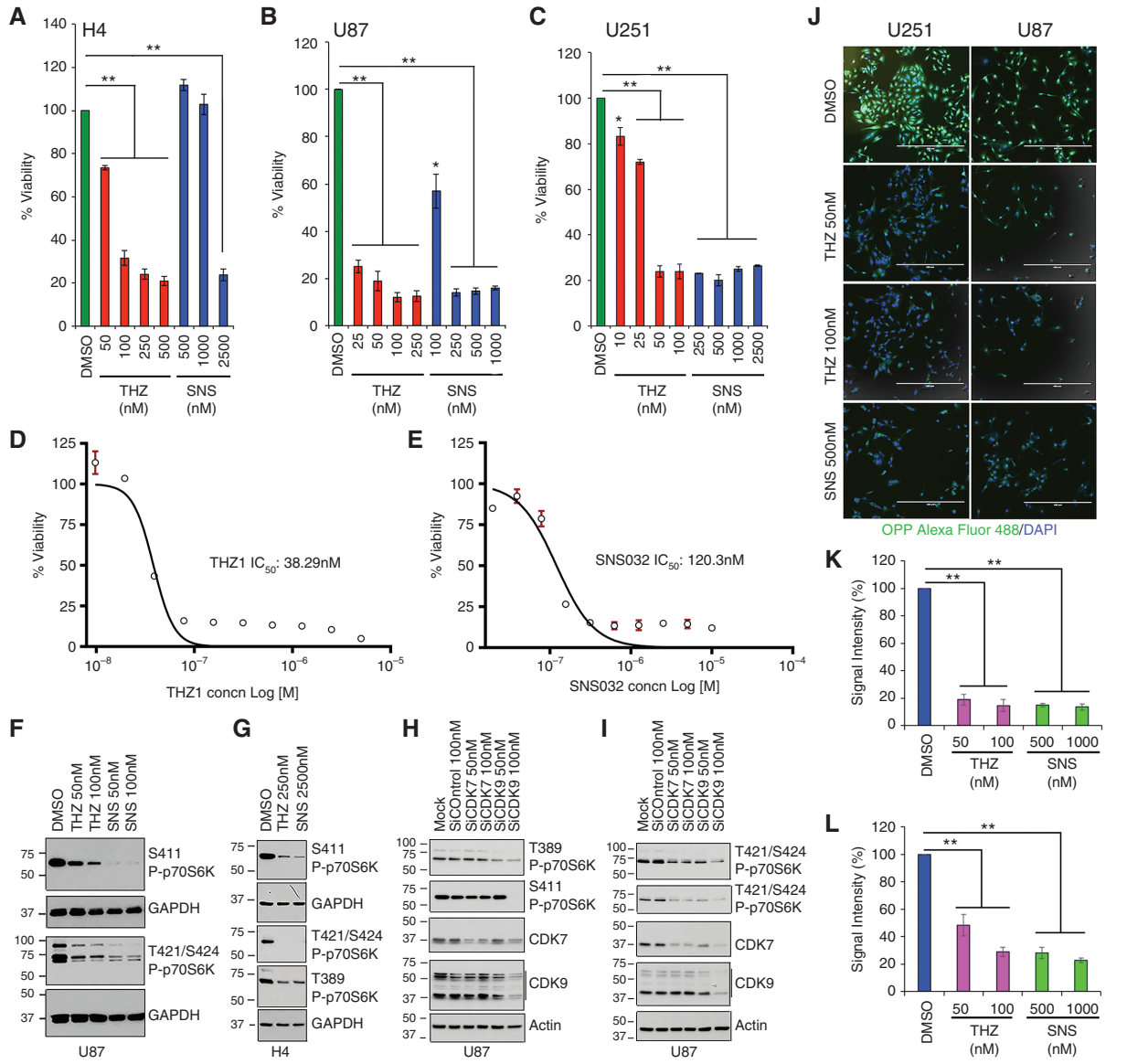

Figure 1. CDK7 and CDK9 inhibitors significantly reduce viability and abrogate p70S6K phosphorylation and protein synthesis in GBM cells. (A–C) Cell viability. H4, U87, and U251 cells treated with THZ1 or SNS032 for 72 hours. *$P < .05$; **$P < .01$. (D, E) IC_{50} analysis showing the potency of THZ1 and SNS032 against U251 cells. THZ1 was tested at a range of 10 nM to 5 μM and SNS032 from 20 nM to 10 μM. (F-I) Western blot analysis (WB). (F, G) Treatment with THZ1 and SNS032 decreased the levels of S411 and T421/S424 P-p70S6K in U87 and H4 cells and P-T389 in H4 cells. GAPDH was used as a loading control. (H, I) Knockdown (KD) of CDK7 or CDK9 by pooled siRNA reduced S411, T389 and T421/S424 phosphorylation on p70S6K in U87 cells, more with siCDK9 than siCDK7; scrambled siRNA was used as a control. Actin was used as a loading control. (J) U251 and U87 cells were treated with THZ1 or SNS032 and nascent protein synthesis was measured by OPP incorporation (green). Nuclei were stained with DAPI (blue); scale bar, 400 μm. (K, L) quantification of nascent protein synthesis in U251 (K) and U87 (L).

THZ1 or SNS032 revealed a marked reduction in p70S6K phosphorylation on multiple sites (T389, S411, T421, and S424). siRNA knockdown (KD) of CDK9, and to a lesser extent CDK7, confirmed that these kinases play a specific role in p70S6K phosphorylation. Compared to control siRNA-treated cells, a decrease in phosphorylation of p70S6K at T389, S411, and T421/S424 epitopes was observed in U87 cells treated with 100 nM CDK9 siRNA, with maximum effect on the phosphorylation of S411 epitope (Figure 1H-I). CDK7 KD cells showed changes mainly in the T421/S424 phospho-p70S6K (Figure 1I). These data suggest that the decrease in p70S6K phosphorylation caused by SNS032, more than THZ1, resulted from inhibition of these CDKs, and not from off-target effects. Since phosphorylation of p70S6K at the above amino acid residues are critical for protein translation, we examined if CDK7 and CDK9 inhibitors suppress protein translation. A nascent protein synthesis assay was conducted using the Click-iT OPP (O-Propargyl-Puromycin) reagent. As shown in Figure 1J to 1L, treatment of U251 and U87 cells with THZ1 and SNS032 significantly reduced OPP incorporation as evidenced by reduced fluorescence intensity (quantified in Figure 1K-L), indicating that these inhibitors suppress p70S6K activity and nascent protein synthesis. We next assessed if an inhibitor of p70S6K enhances the efficacy of THZ1 and SNS032 on GBM cells and found that M2698, a dual inhibitor of p70S6K and Akt, could cooperate to a certain extent with THZ1 and SNS032 to reduce the viability of U251, U87, and H4 cells (Supplementary Figure 1 A-C).

p70S6K Inhibitor Enhanced Akt and ERK Phosphorylation in GBM Cells

Next, we examined whether M2698 cooperates with THZ1 or SNS032 to attenuate p70S6K phosphorylation in GBM cells. U87 and U251 cells treated with SNS032 for 24 hours showed a strong decrease in S411 but a weak effect on T421/S424 phospho-p70S6K. THZ1 had only a marginal effect at the concentration tested (Figure 2A). M2698 treatment alone reduced p-T421/S424 levels, and this was further reduced when it was combined with THZ1 or SNS032 (Figure 2A and B). Treatment with THZ1 and SNS032 showed only marginal reduction in p70S6K phosphorylation in H4 cells. However, when combined with M2698, SNS032 markedly reduced the phosphorylation at S411 but not at T421/S424 sites, whereas THZ1 mainly reduced phospho-T421/S424 (Figure 2C). Levels of phospho-Pol II were also reduced with SNS032 treatment in U87 and U251 cells but not H4, at the concentrations tested; this correlates with the cell viability analysis, which showed that H4 cells require higher doses of THZ1 and SNS032 for complete growth suppression (Figure 1; Supplementary Figures 1 and 2).

Since M2698 is known to inhibit both Akt and p70S6K,[39] we examined the levels of Akt phosphorylation in the cells by reprobing the blots with the Pathscan Western Cocktail 1 antibodies. Surprisingly, M2698 treatment led to an increase in the levels of phospho-Akt in the GBM cells (Figure 2A-C, bottom rows). Additionally, phospho-ERK was also increased in M2698-treated U87 and H4 cells, implying that treatment with this agent alone may enhance both proliferation and survival-associated signaling in GBM cells. This activation of Akt and ERK by M2698 may be the reason for its lack of single-agent impact on the GBM cell viability we observed. The mechanisms driving the activation of ERK and Akt are unclear at this point. Despite ERK and Akt activation, M2698 additively inhibited cell viability when combined with THZ1 or SNS032 (Supplementary Figures 1 and 2). Probing with the cocktail antibody also showed a complete loss of p-S6 (Figure 2A-C, bottom panels labeled Pathscan), confirming that p70S6K activity is indeed inhibited upon M2698 treatment. Reprobe of the blots also showed that THZ1 and SNS032 as single agents or in combination with M2698 show nominal increase in PARP cleavage in U87 and H4 cells 24 hours after treatment (Figure 2A-C).

Given the reduction in cell viability, BrdU incorporation assays were conducted to assess if the inhibitors affected cell proliferation. U251 and U87 cells treated with 100 nM THZ1 or 500 nM SNS032 showed a significant reduction in BrdU incorporation (Figure 2D-F). Furthermore, cell-cycle analysis conducted on U87 and the intrinsically TMZ-resistant T98G cells revealed that treatment with 500 nM SNS032 or 25 nM AZD4573, a more potent CDK9 inhibitor, for 24 and 48 hours resulted in G2 arrest (Figure 2G-H; Supplementary Figure 3), suggesting that the transcriptional inhibitors attenuate proliferation and induce mitotic arrest prior to induction of apoptosis.

THZ1 and SNS032 Inhibit Cell Migration and Anchorage-Independent Growth of GBM Cells

The effect of CDK7 and CDK9 inhibitors on the migration and anchorage-independent growth of H4 and U251 cells was examined. THZ1 and SNS032 reduced the migration of the cells effectively (Figure 2I, 2K); combining with M2698 did not elicit an additive effect at the doses tested (Figure 2J-K). Analysis of anchorage-independent growth by soft agar assay showed a significant, concentration-dependent, reduction in colony formation in both U87 and H4 cells (Figure 2L). M2698 alone markedly reduced colony formation in H4 cells, which was further reduced when combined with THZ1 or SNS032 (Supplementary Figure 4 A-C); such an added effect was not observed in U87 cells, indicating that each GBM cell line responds to the inhibitors differently, despite the major shared mutations in these cells.

TMZ-Resistant GBM Cells are Responsive to THZ1 and SNS032 Treatment

Since a major challenge in GBM treatment is TMZ resistance, we tested whether CDK inhibitors could abrogate the growth and oncogenic characteristics of TMZ-resistant cells. Treatment with 100 nM THZ1 or 500 nM SNS032 significantly reduced the viability of TMZ-resistant U251 (U251R) cells, indicating that these CDK inhibitors can eliminate GBM cells that are resistant to TMZ (Figure 3A). Additionally, nanomolar concentrations of THZ1 and SNS032 markedly reduced the levels of phospho-Pol II and phospho-p70S6K in U251R cells, comparable to parental U251 cells. These changes did not occur in cells that were

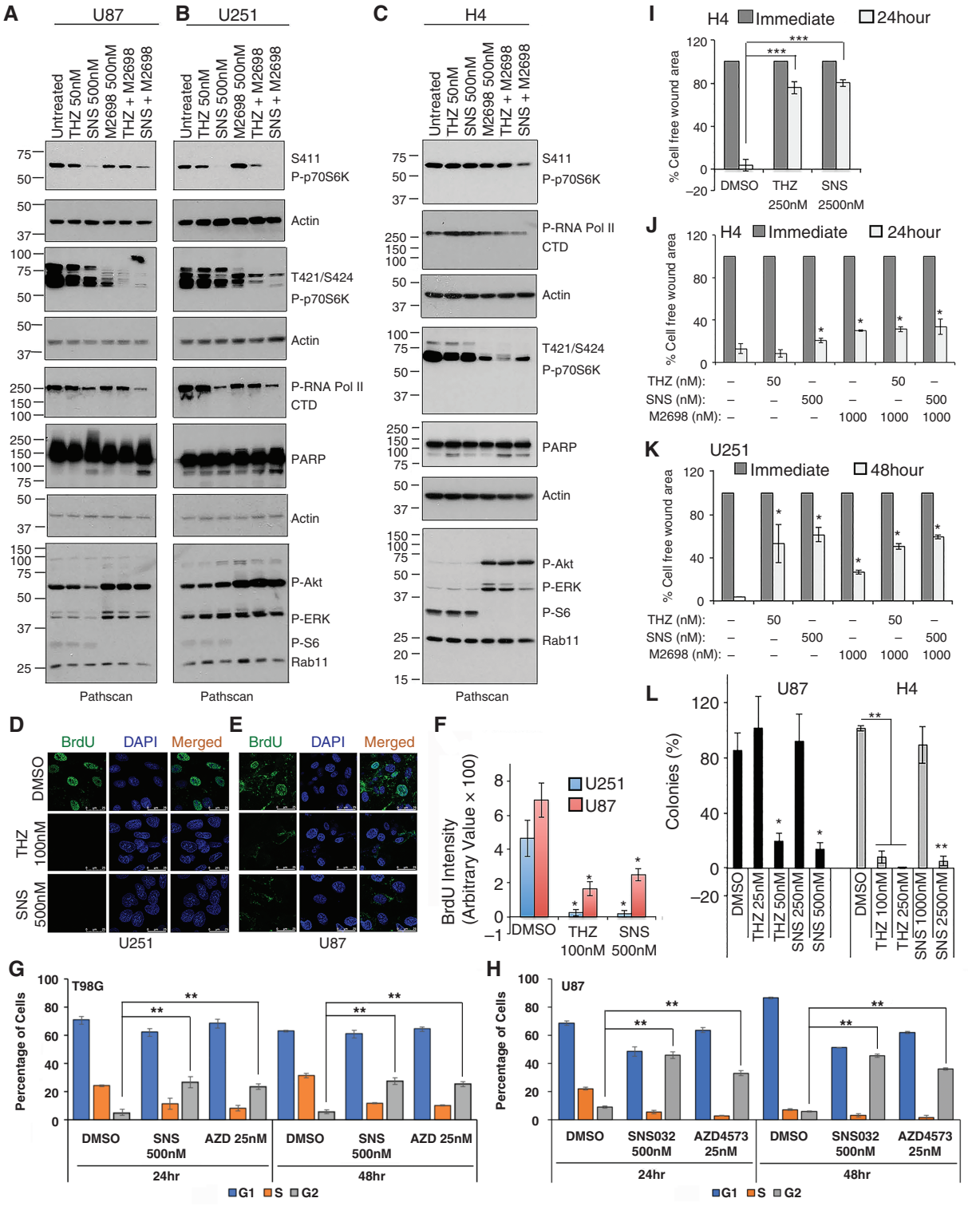

Figure 2. M2698 inhibits p70S6K but enhances Akt and ERK phosphorylation: (A—C) WB for S411 and T421/S424 P-p70S6K, P-Akt, and P-ERK in U87 (A), U251 (B), and H4 (C) cells treated with THZ1, SNS032 or M2698, alone or in combination. (D–E) Immunofluorescent Staining (IF) for BrdU incorporation in U251 and U87 cells treated with THZ1 or SNS032 (green—BrdU, blue—DAPI), scale bar, 25 μm; F: Quantification of BrdU positive cells. (G-H) FACS for cell-cycle analysis on T98G (G) and U87 (H) cells treated with 500 nM SNS032 or 25 nM AZD4573 for 24 or 48 hours. Y axis shows the percentage of cells in G1, S or G2 phase of cell cycle. (I-K) Wound healing assay for H4 and U251 cells, in the presence of THZ1, SNS032 or M2698 for 24 or 48 hours. Cell migration was assessed by measuring the area of the wound. L: Soft agar assay quantification for the number of colonies formed by U87 and H4 cells treated with THZ1 or SNS032.

only treated with 100 μM of TMZ (Figure 3B). Consistent with these results, THZ1 and SNS032 suppressed the anchorage-independent growth of both U251 and U251R cells in soft agar (Figure 3C-D), while treatment with TMZ inhibited colony formation only in TMZ-responsive U251 cells.

3D spheroids are considered as better model system than 2D cultures for drug efficacy studies in cancer. We generated spheroids from U251, U87-GFP, and H4 cells by growing them in serum-free DMEM/F12 containing EGF, bFGF, and N2 supplements; treatment with THZ1, SNS032 or M2698 for 10 days reduced the spheroid formation,

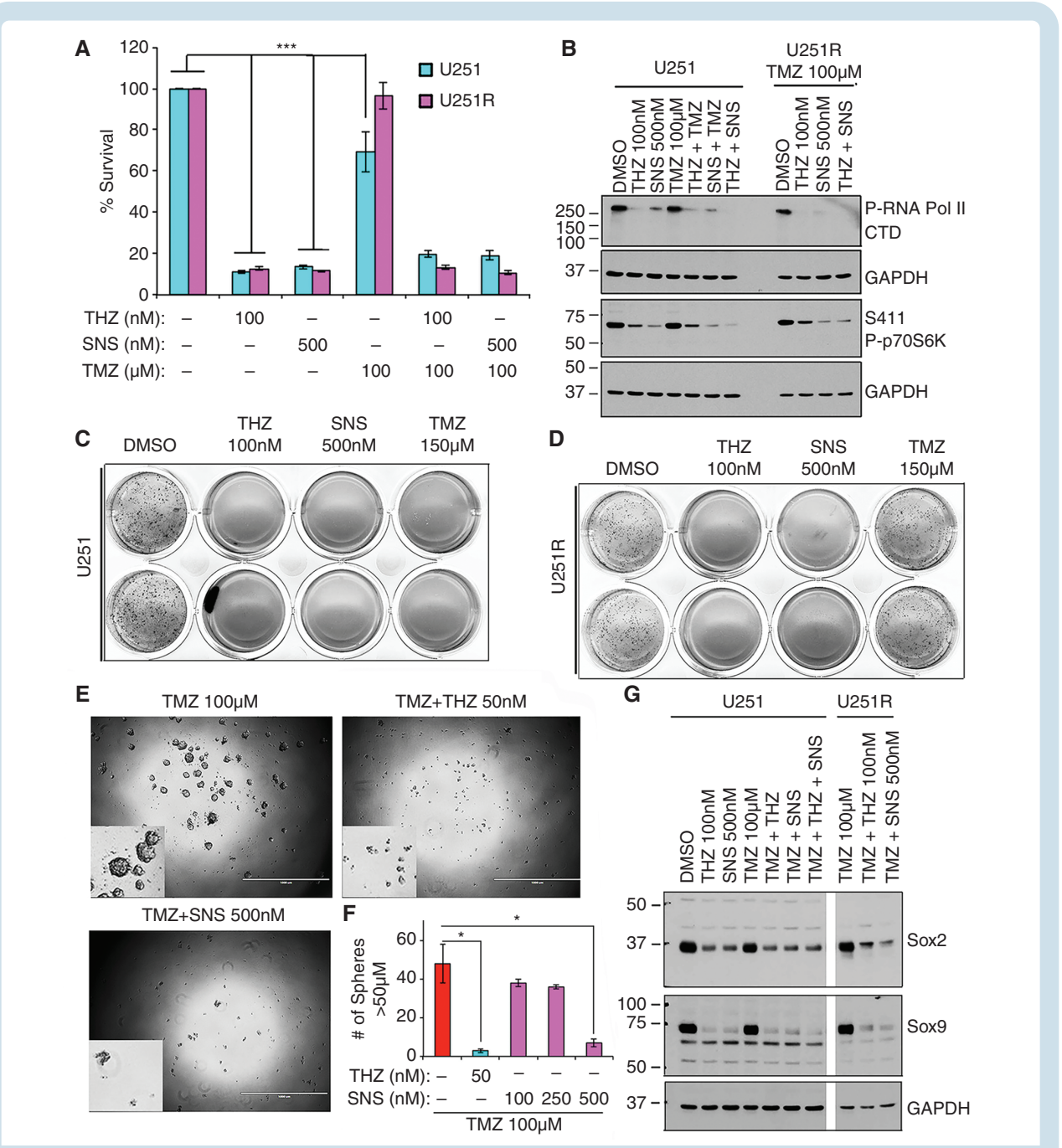

Figure 3. TMZ-resistant GBM cells are responsive to THZ1 and SNS032: (A) MTT assays. TMZ-responsive (U251) and resistant (U251R) cells were equally sensitive to THZ1 and SNS032. (B) WB for P-Pol II and P-p70S6K in U251 or U251R cells treated with TMZ (100 μM) THZ1 (100 nM), or SNS032 (500 nM). (C, D) Soft agar assays for U251 or U251R cells treated with THZ1, SNS032 or TMZ at indicated doses. (E) Inhibition of glioma spheroid growth in U251R cells upon treatment with TMZ, TMZ + THZ1 or TMZ + SNS032 at indicated doses; scale bar, 1000 μm. (F) Quantification of spheres larger than 50 μm. (G) WB for Sox2 and Sox9 expression in U251 or U251R cells treated with THZ1, SNS032 or TMZ individually or at the indicated combinations.

indicative of the ability of the drug to interfere with the growth of non-adherent spheroids; M2698 was less effective as a single agent (Supplementary Figure 5 A-F). Similarly, while the resistant U251R cells continued to form spheres in the presence of TMZ, spheroid formation was suppressed by THZ1 and SNS032 (Figure 3E-F). At molecular level, THZ1 and SNS032 markedly reduced the levels of Sox2 and Sox9 in both TMZ-responsive and resistant GBM cells, but not in cells treated with TMZ alone (Figure 3G; Supplementary Figure 6). Taken together, CDK7 and CDK9 inhibitors effectively suppress the growth and stem-like characteristics of GBM cells that are refractory to TMZ.

Expressions of CDK7, CDK9, SOX2, SOX9, and RP6KB1 are Altered in Clinical Gliomas

Analysis of the expression correlations among CDK7, CDK9, SOX2, SOX9, and RPS6KB1 in the TCGA GBM gene expression dataset (http://firebrowse.org/) showed a significant correlation between SOX2 and SOX9 ($r = 0.41$, $P < .001$) (Figure 4A-B). Furthermore, comparative analysis showed that SOX2 and SOX9 expression were significantly higher in glioma patient samples compared to the normal brain (Figure 4C-D; 502 glioma tumors and 10 normal samples), which might contribute to the maintenance of the GSC population and resistance development. CDK7 or CDK9 expression were not significantly altered but the levels of RPS6KB1 were elevated (Figure 4E). To further validate the observations from TCGA dataset, we conducted a multispectral imaging on a GBM TMA (GL806f, US Biomax, Inc.), and assessed the expression levels of CDK7, CDK9, Sox2, Sox9, and phospho-p70S6K; GFAP was used as tumor marker. We observed increased expression of CDK9, Sox2, and Sox9 in the GBM cores compared to the normal brains (Figure 4F-H); CDK7 levels also showed a significant increase in the GBM cores, but to a lesser extent. The phospho-p70S6K antibody did not work in the multispectral imaging, but IHC showed a significant increase in its levels in the GBM samples (Supplementary Figure 7 A-B); similarly, phospho-S6 showed a marked increase by IHC in the GBM samples (Supplementary Figure 7C). Taken together, these data suggest that CDK9, Sox2, Sox9, and p70S6K might contribute to GBM tumorigenicity and their suppression would negatively impact GBM growth.

CDK7 and CDK9 Inhibition Suppressed Growth of Patient-Derived GSCs, Primary GBM Cells as Well as PDX-Derived Cells

Given the results from the TMAs, we expanded our studies to patient-derived GBM cells and GSCs. Three previously characterized GSCs (GSC576,[31] GSC1478,[32] and GBM6[33]) were treated with varying concentrations of THZ1 or SNS032 for 96 hours; both THZ1 and SNS032 significantly reduced the viability of GSCs at nanomolar concentrations (Figure 4I-K). THZ1 (100 nM) and SNS032 (500 nM) also reduced the phosphorylation of Pol II and p70S6K in the GSCs (Figure 4L); THZ1 showed only a mild effect on the phospho-p70S6K in GSC576. Expression of Sox2 and Sox9 as well as levels of total ERK were reduced upon treatment with SNS032 in all the three GSCs, while THZ1 showed effect mainly in GSC1478 (Figure 4L). Treatment of these GSCs, as well as, patient-derived TMZ-responsive (GBM42WT) and resistant (GBM42R) cells, and GBM43 PDX cells, with additional CDK9 inhibitors (LY2857785, AZD4573, NVP2, or JSH150) showed that these agents, especially AZD4573 and NVP2, induce significant cytotoxicity at very low nanomolar concentrations (Figure 4M; Supplementary Figure 8). These results suggest that CDK9 inhibition can eliminate TMZ-insensitive GBM cells as well and maybe a viable option for treating GBM.

CDK9 Inhibition Interferes With Invasiveness, Anchorage-Independent Growth, and Self-Renewal of Patient-Derived, TMZ-Responsive and Resistant, GBM Cells

Since GBM tumors are highly invasive, next we examined if CDK9 inhibitors interfere with invasion of the tumor cells. Boyden chamber assays conducted with GBM42WT and GBM42R cells showed that treatment with 500 nM SNS032 or 50 nM AZD4573 significantly reduce their invasion (Figure 4N). Similarly, a soft agar colony formation assay showed that 25 nM AZD4573 and 250 nM SNS032 interfere with the anchorage-independent growth of both TMZ-responsive and resistant GBM42 cells (Figure 4O); treatment with 50 nM AZD and 500 nM SNS032 completely eliminated the colony formation. Furthermore, AZD4573 and NVP2 could suppress self-renewal and sphere-forming capability of both GBM42WT and GBM42R cells even at 10 nM concentration, while 25nM completely eliminated the spheres (Figure 4P). Altogether, these data clearly show that CDK9 inhibitors have the potential to inhibit the growth of GBM cells and GSCs.

Genes Associated With Tumor Suppressive Pathways are Upregulated in GBM Cells Treated With THZ1 and SNS032

To further understand the pathways affected by these CDK inhibitors, we analyzed the global gene expression profiles in U87 and U251 cells treated with THZ1 (100 nM) or SNS032 (500 nM) for 24 hours, by RNA-Seq. Significant changes were found in both U87 and U251 cells (Figure 5A-B and Supplementary Figure 9 A-D); overlapping and differential regulation of several genes were observed (Supplementary Figure 9 A-B). Hypergeometric test showed that both overlaps were highly significant ($P < 10^{-6}$). A *REACTOME* pathway analysis using the dataset from RNA-seq showed alterations in several pathways, including those involved in cell cycle, chromatin remodeling, and p53-associated transcriptional regulation (Figure 5C-D). Expression of several genes involved in neuronal activity, plasticity, tumor suppression, cell-cycle arrest, cell differentiation, DNA damage and/or apoptosis, etc., such as EGR1, ARC, GADD45A, GADD45B, and CDKN1C, were increased upon inhibition of CDK7 and CDK9, suggesting potential mechanisms by which these inhibitors abrogate GBM growth. Moreover, these data also imply that CDK7/9 inhibition might not adversely affect differentiated neurons but rather complement their normal functioning.

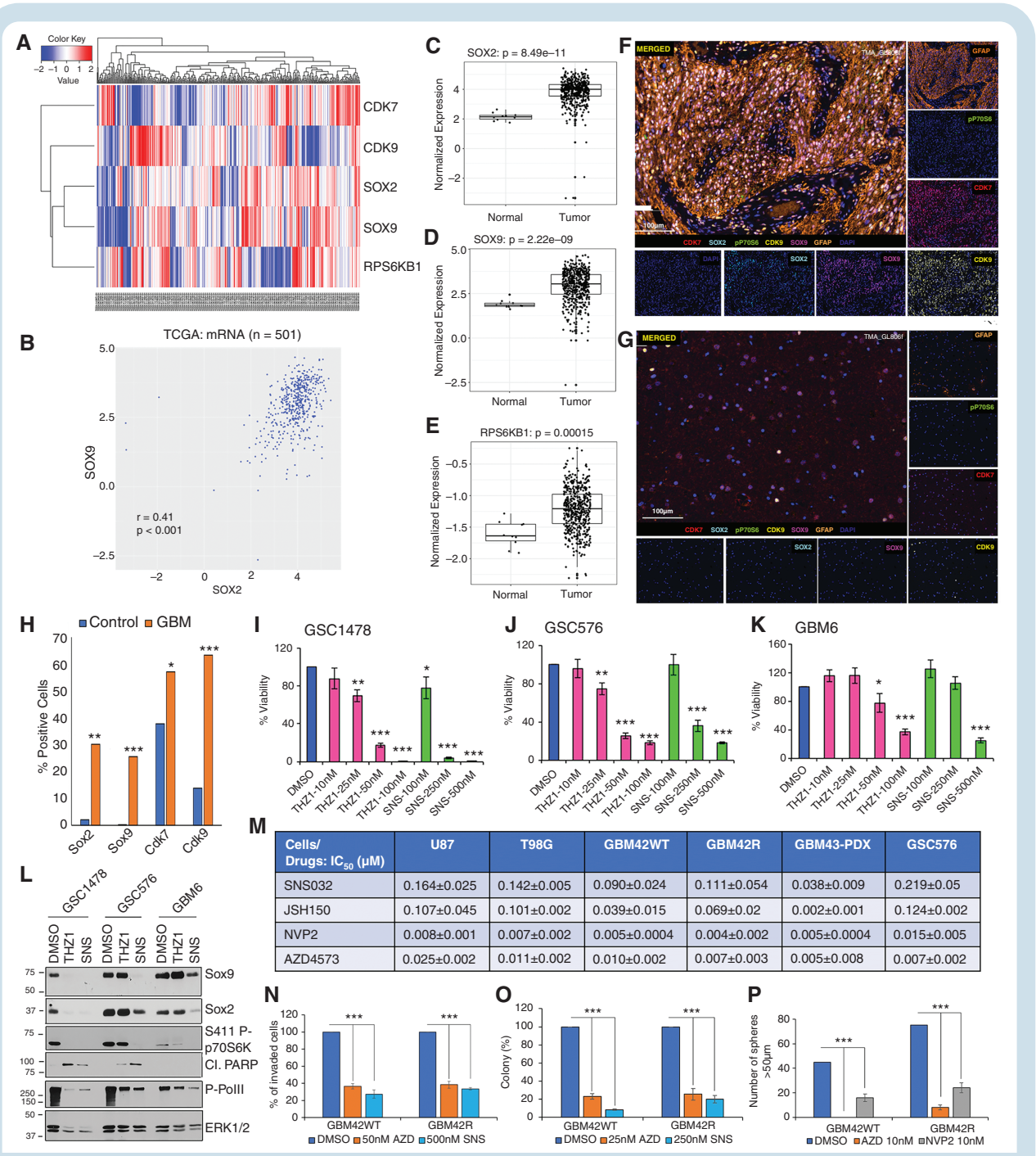

M

Cells/ Drugs: IC_{50} (μM)	U87	T98G	GBM42WT	GBM42R	GBM43-PDX	GSC576
SNS032	0.164±0.025	0.142±0.005	0.090±0.024	0.111±0.054	0.038±0.009	0.219±0.05
JSH150	0.107±0.045	0.101±0.002	0.039±0.015	0.069±0.02	0.002±0.001	0.124±0.002
NVP2	0.008±0.001	0.007±0.002	0.005±0.0004	0.004±0.002	0.005±0.0004	0.015±0.005
AZD4573	0.025±0.002	0.011±0.002	0.010±0.002	0.007±0.003	0.005±0.008	0.007±0.002

Figure 4. Alterations in CDK9, SOX2, SOX9 and RPS6KB1 gene expression in clinical GBM samples and responses of patient-derived glioma stem cells and GBM cells to THZ1 and CDK9 inhibitors: (A-B) Relative gene expression (z-score) across TCGA glioma samples and correlation analysis for co-expression of SOX2 and SOX9. (C–E) Normalized expression values showed significantly elevated levels of SOX2 (C), SOX9 (D), and RPS6KB1 (E) in the TCGA gliomas compared to the normal samples. F–H: Multiplex imaging analysis on a GBM TMA showed increased expression of Sox2, Sox9, CDK9 and a lesser increase in CDK7 in the tumor (F) compared to normal (G) brain tissues. GFAP was used as the tumor marker and DAPI for the nuclei; scale bar, 100 μm. (H) Quantification from the TMA. I-K: CellTiter-Glo assays on three different glioma stem cells. GSC1478 (I), GSC576 (J), and GBM6 (K) spheres treated with varying concentrations of THZ1 or SNS032. (L) WB for P-Pol II, S411 P-p70S6K, Sox2, and Sox9 in GSCs treated with 100 nM THZ1 or 500 nM SNS032. M: IC_{50} values of cell viability for U87, T98G, GBM42WT, GBM42R, GBM43 PDX, and GSC576 treated with 10 different concentrations of SNS032, JSH150, NVP2, or AZD4573 for 72 hours. N: Matrigel invasion assay. GBM42WT or GBM42R cells were plated in Boyden chamber and treated with 500 nM SNS032 or 50 nM AZD4573 and the invaded cells were quantified. O: Soft agar colony formation assay for GBM42WT and GBM42R cells treated with 25 nM AZD4573 or 250 nM SNS032. P: Self-renewal capacity of GBM42WT and GBM42R cells treated with 10 nM AZD4573 or 10 nM NVP2.

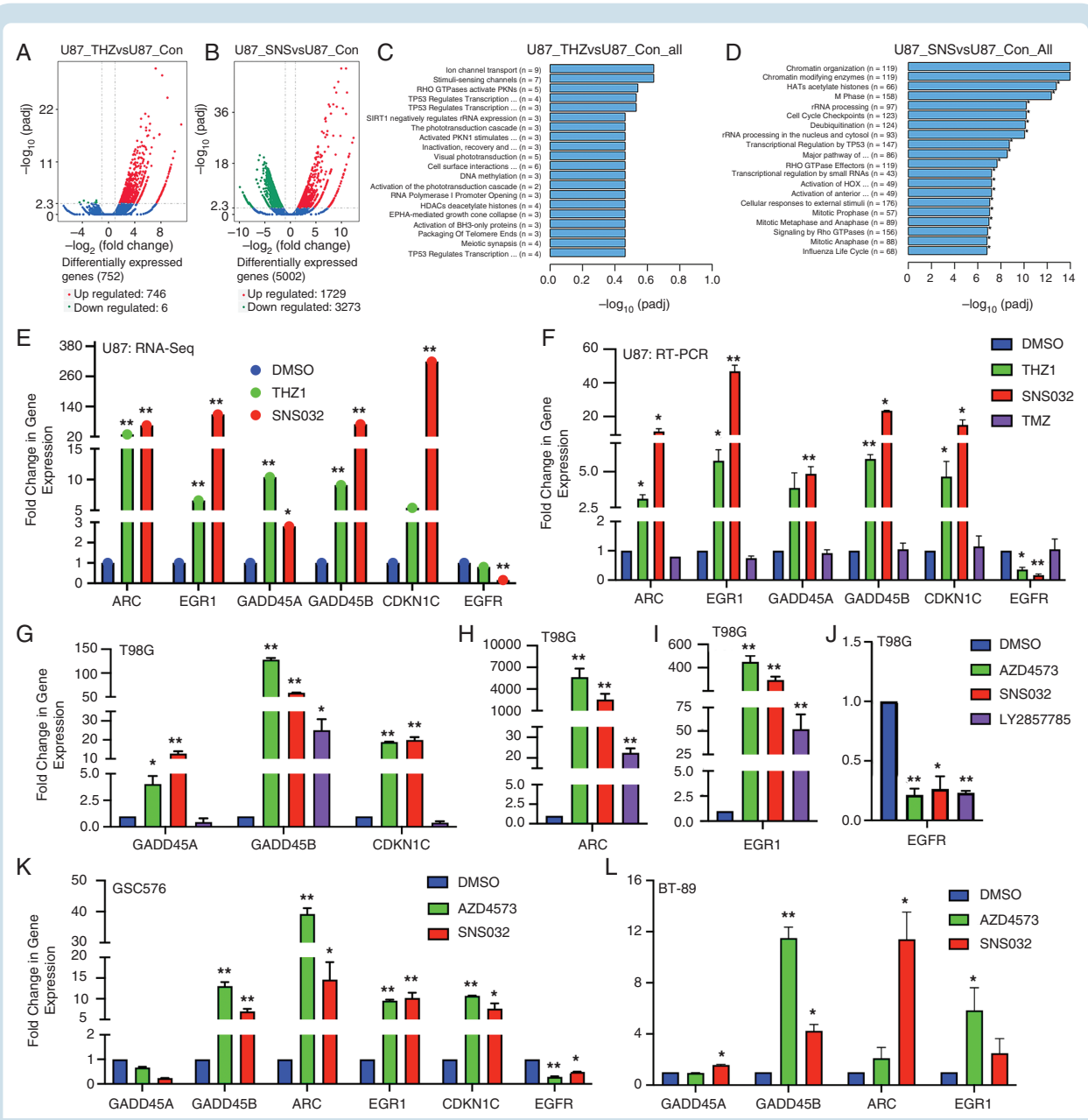

Figure 5. Simultaneous activation and inhibition of tumor suppressive and tumor promoting pathways in CDK7 and CDK9 inhibitor treated GBM cells. (A-B) Volcano plots from U87 cells treated with 100 nM THZ1 or 500 nM SNS032 for 24 hours. (C–D) *REACTOME* pathway analysis using the RNA-seq dataset from U87 cells treated with THZ1 or SNS032 show alteration in several signaling pathways. (E) Expression changes in a selected set of genes in U87 cells treated with 100 nM THZ1 or 500 nM SNS032 for 24 hours, taken from RNA-seq dataset. (F) RT-PCR analysis confirmed the changes observed by RNA-seq in U87 cells. Data from cells treated with THZ1 (100 nM), SNS032 (500 nM) or TMZ (100 μM). (G–L) RT-PCR analysis for changes in expression of the indicated genes in intrinsically TMZ-resistant T98G cells (G–J), GSC576 (K) or GSC BT89 (L) cells, treated for 24 hours with the indicated CDK9 inhibitors (500 nM SNS032, 500 nM LY2857785 or 50 nM AZD4573).

A subset of genes that showed altered expression in the treated GBM cells were validated by RT-PCR. The expression of EGR1, ARC, GADD45A, GADD45B, and CDKN1C were elevated in U87, U251, and U251R cells treated with the CDK7/9 inhibitors whereas that of EGFR was decreased (Figure 5 E-F, and Supplementary Figure 9 E-H).

Furthermore, studies conducted on various GBM cells and GSCs (T98G, U87, GSC576, BT89, GBM42WT, GBM42R, and GBM43 PDX line), treated with additional CDK9 inhibitors [SNS032 (500 nM), AZD4573 (20 nM), LY2857785 (500 nM), NVP2 (25 nM), and JSH150 (150 nM)] showed similar changes in gene expression patterns, analogous to that observed in U87 and U251 cells treated with SNS032 (Figure 5 G-L and Supplementary Figure 10 A-E). These data predict that CDK9-targeted therapies would bring about the anti-tumor activity by promoting tumor suppressive mechanisms in the cells within the highly heterogeneous GBM tumor, irrespective of their

sensitivity to TMZ. Analysis conducted on primary rat cortical neurons showed that treatment with THZ1 or SNS032 did not drastically affect their viability (Supplementary Figure 11), even at concentrations higher than that was required for significant cytotoxicity induction in TMZ-sensitive and resistant GBM cells and GSCs (Figure 1A-C; Figure 3A; Figure 4I-K). Thus, these results further suggest the therapeutic potential of CDK7 and CDK9 inhibitors in suppressing GBM without eliciting cytotoxicity in post-mitotic neurons.

CDK9 Inhibitor Treatment Shows a Time-Dependent Decrease in Phosphorylation of p70S6K and Pol II and Markedly Reduced the Expression of Mcl1 in GBM Cells and GSCs

Since CDK7 and CDK9 inhibitors elicited significant cytotoxic effects at low nanomolar concentrations, we conducted a time course analysis for changes in phospho-p70S6K and phospho-Pol II in GBM42WT and GBM42R cells treated with 50 nM AZD4573. Phosphorylation of p70S6K at S411 was decreased within 3 hours of inhibitor treatment (Figure 6A) whereas that at T421/S424 was decreased only after 24 to 48 hours (Figure 6A). Similarly, phospho-Pol II also decreased within 3 hours after AZD4573 treatment, and it continued to decrease during the time course (Figure 6B). Total levels of p70S6K and Pol II were not affected at the early time points but were decreased by 24 hours. Quantification of the WB data showed that the phosphorylation on S411-p70S6K and S2-Pol II remained significantly low at all the tested time points (Figure 6C-E). Interestingly, AZD4573 treatment led to a decrease in the levels of Mcl1, a target of CDK9, that is known for its anti-apoptotic function and contribution to drug resistance (Figure 6B, row 3). Supporting this, both WT and resistant GBM42 cells showed a time-dependent increase in PARP cleavage indicative of induction of apoptosis in response to the treatment (Figure 6A, row 4). Similarly, the levels of Sox9 were also decreased in a time-dependent fashion upon treatment with AZD4573 (Figure 6B, row 4).

Similar observations were made with GSC576 and T98G cells, treated with 100 nM THZ1, 500 nM SNS032, or 50 nM AZD. Here also we observed a decrease in the levels of S411-phospho-p70S6K and S2-phospho-Pol II within 2 hours of inhibitor treatment (Supplementary Figure 12 A-B). Besides, THZ1 showed less effects on these epitopes. This agrees with our data from the knockdown studies, where we observed a drastic decrease in S411-phospho-p70S6K in siCDK9 KD cells compared to that in siCDK7 (Figure 1H). T421/S424 phospho-p70S6K showed a time-dependent reduction with THZ1 in GSC576 but the reduction was visible only after 24 hours treatment with CDK9 inhibitors (Supplementary Figure 12 A). Moreover, total protein levels of p70S6K and Pol II were not affected at the earlier time points but were decreased at 24 hours. Additionally, treatment with SNS032 and AZD4573 led to a time-dependent decrease in the levels of Mcl1 and an increase in PARP cleavage (Supplementary Figure 12 A-B, rows 5 and 6 from the top), as in GBM42 cells. Lastly, THZ1 did not affect Mcl1 expression markedly, indicating the specificity of the CDK9 inhibitors towards Mcl1.

AZD4573 and SNS032 Suppressed the Growth of GSC576 Subcutaneous Tumor Xenografts

To test if the CDK9 inhibitors can suppress growth of GSC-derived tumor xenografts in vivo, we implanted GSC576 cells into the flanks of athymic nude mice. The tumor xenografts were allowed to reach ~100 mm^3 before administering SNS032 or AZD *via* i.p. at 15 mg/kg. Both SNS032 and AZD significantly reduced the growth of GSC576 tumor xenografts in vivo (Figure 6F-H). Although AZD showed higher inhibitory effects in vitro at much lower concentrations, our in vivo data were comparable between the SNS032 and AZD treatments.

SNS032 Inhibits Tumor Growth in an Orthotopic GBM Xenograft Model:

To assess the efficacy of SNS032 on GBM orthotopic growth in the brains of animals, we conducted an experiment on SCID mice using U251-luc cells. SNS032 was delivered intratumorally as a continuous infusion for 4 weeks using an Alzet osmotic pump. The inhibitor was well tolerated, and the mice did not show any weight loss over the course of the study. In vivo, imaging showed a marked reduction in the growth of orthotopic tumor xenografts in the mice receiving SNS032 compared to the vehicle group (Figure 6I-K). A Kaplan–Meier analysis showed that SNS032 treatment markedly extended the life span of the tumor-bearing mice compared to the vehicle-treated animals (Figure 6L). Taken together, our preclinical studies from the orthotopic and subcutaneous xenograft models suggest that targeting CDK9 would be a potential therapeutic strategy to treat GBM with tolerable toxicity.

Discussion

Attempts to effectively treat GBM have been hampered by several challenges, including high tumor heterogeneity, intrinsic resistance to therapies, inevitable tumor recurrence as well as neurotoxicity of the agents. The results reported here suggest that targeting CDK7 and/or CDK9 would effectively suppress the growth of TMZ-responsive and -resistant GBM with low neurotoxicity.

CDK7 and CDK9 play important roles in gene expression through phosphorylation and regulation of Pol II.[40,41] We find that in addition to inhibiting transcription, CDK7, and CDK9 inhibitors block p70S6K, a kinase known for its role in protein translation and poor prognosis in cancer patients.[42,43] The simultaneous inhibition of Pol II and p70S6K by the CDK7/9 inhibitors highlight the ability of these agents to target multiple signaling cascades to suppress tumor growth.

This study also reveals a potential mechanism that renders GBM cells resistant to p70S6K inhibitors. Targeting of mTOR and p70S6K signaling in cancers, including GBM, have met with limited success; our results suggest that the lack of efficacy might be caused by the compensatory activation of ERK and Akt pathways. In this context, our finding that CDK7 and CDK9 inhibitors induce cytotoxicity, irrespective of the higher levels of phospho-Akt and phospho-ERK in M2698 treated GBM cells, is encouraging and is of

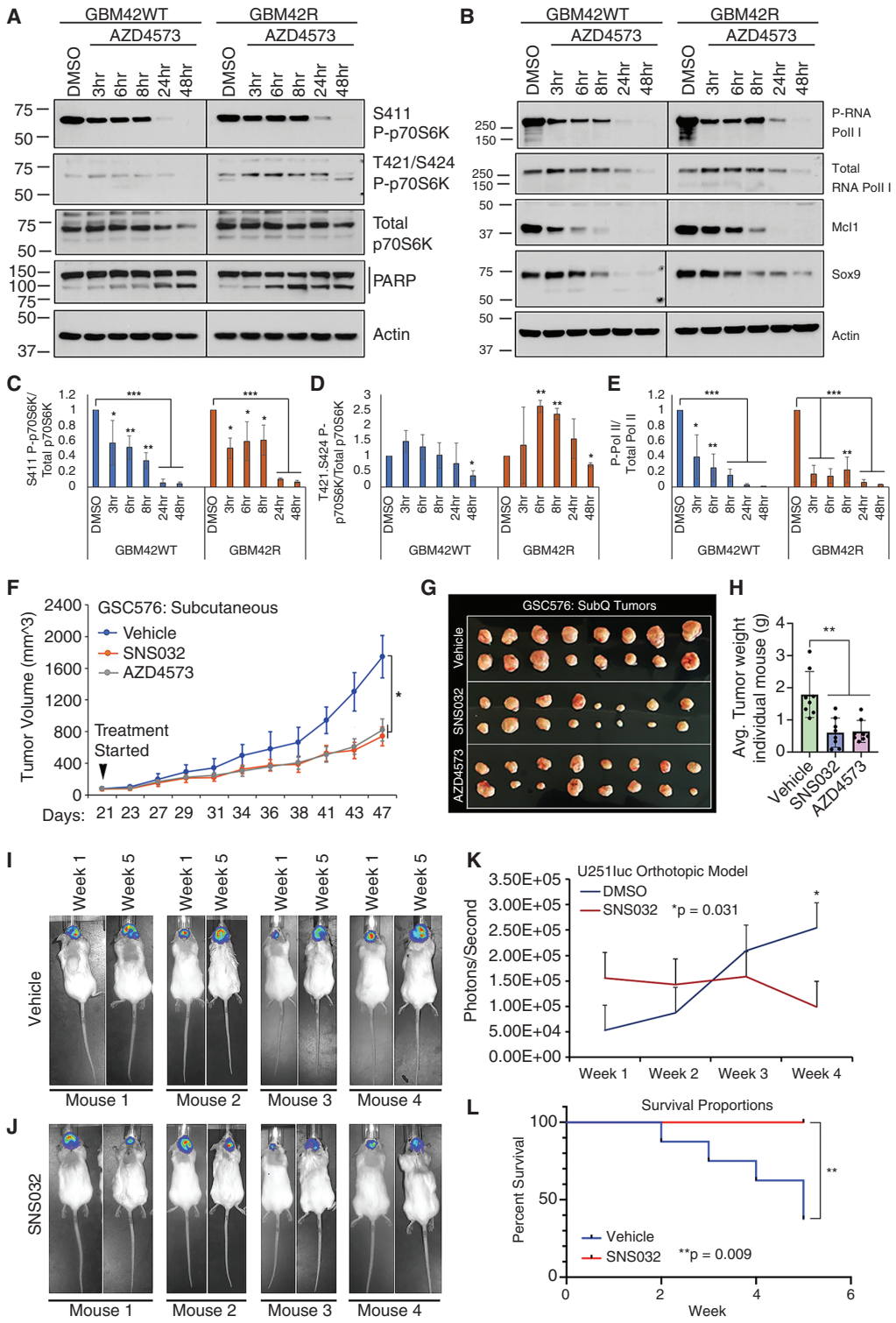

Figure 6. CDK9 inhibitors suppress the expression of Mcl1 in GBM cells and abrogate the tumor growth in xenograft models: (A-B) WB for a reduction in P-p70S6K, P-Pol II, Mcl1, Sox9 and an increase in PARP cleavage in GBM42WT and GBM42R cells treated with 50 nM AZD4573 for indicated times. Total p70S6K, total Pol II and actin are loading controls. C–E: Ratio of S411 P-p70S6K (C), T421/S424 P-p70S6K (D) or P- Pol II (E) to, total p70S6K or total Pol II, respectively. (F–L) CDK9 inhibition suppresses tumor growth in GBM xenograft models. F: SNS032 and AZD4573 treatment inhibited growth of GSC576 subcutaneous xenografted tumors. (G, H) The excised tumors and average tumor weight from each mouse. (I-K) Bioluminescence images from SCID mice orthotopically implanted with U251-luc cells treated with vehicle (I) or SNS032 (10 mg/kg) (J) using Living Image software; SNS032 treatment reduced tumor growth as assessed by bioluminescent imaging (K). L: Kaplan–Meier analysis for survival of brain tumor-bearing mice treated with vehicle or SNS032.

clinical relevance. Furthermore, the cytotoxicity of CDK7 and CDK9 inhibitors were not hampered by ERK or Akt activation, indicating their ability to override these survival pathways. One such pro-apoptotic mechanism could be the suppression of the anti-apoptotic Mcl1 and the activation of PARP cleavage by CDK9 inhibitors.

The ability of the CDK7/9 inhibitors to sensitize TMZ-resistant GBM cells is another significant result in this study. The fact that GSCs and the patient-derived,TMZ-responsive and -resistant, GBM cells displayed high sensitivity to the CDK9 inhibitors signifies the potential applicability of these agents to combat treatment refractory GBM. The finding that the CDK9 inhibitors enhance tumor suppressive pathways while simultaneously suppressing oncogenic genes demonstrates a unique mechanism by which these agents induce growth suppression. In this regard, the knowledge that CDK9 inhibition re-activates epigenetically silenced tumor suppressor genes to bring about anti-tumor activity is notable.[44] CDK9 inhibitors enhanced the expression of growth suppressive ARC, EGR1, GADD45A, GADD45B, and suppressed the expression of proliferative genes such as EGFR, cyclins, and CDKs (data not shown); it is not clear whether epigenetic mechanisms play a role in regulation of their differential expression. EGR1 can enhance or suppress tumor growth in a context-specific manner; we find that increased EGR1 expression correlates with decreased survival implying its role as a tumor suppressor in GBM cells and GSCs. Both EGR1 and its target ARC, another immediate early gene, are implicated in brain development and neuronal plasticity through various mechanisms, including modulation of brain methylome.[45–48] Induction of EGR1 and ARC might be one mechanism contributing to the neuroprotection conferred by CDK9 inhibitors. Similarly, GADD45, which is induced upon CDK9 inhibition, could also be contributing to the neuronal function as it has been shown to play a role in epigenetic gene regulation and neuronal plasticity.[49,50] The absence of severe neurotoxicity, combined with the remarkable growth suppressive properties on GBM cells, strongly indicate that CDK7 and CDK9 are attractive therapeutic targets in GBM and the inhibitors of these kinases might have the potential for reduced cognitive impairment in the patients.

In essence, targeting multiple pathways simultaneously might be beneficial in combating GBM since this approach will probably decrease the activation of compensatory pathways. CDK7 and CDK9 inhibitors seem to fall into this category. Furthermore, as these inhibitors have shown efficacy in treating hematological malignancies, adapting them to treat GBM would be easier. A limitation of these compounds is that they have low permeability across the blood-brain barrier (based on an MDCK-MDR1 analysis) and therefore optimization of these inhibitors for improved brain penetration, or reformulation for direct brain delivery, is warranted for clinical application.

Conclusion

Our results suggest that targeting CDK7 or CDK9 is a viable strategy to suppress the growth and self-renewal of GBM, with low risk of neurotoxicity. It is plausible that these inhibitors could be effective against GBM as single agents or in combination with current standard of care.

Supplementary material

Supplementary material is available online at *Neuro-Oncology* (http://neuro-oncology.oxfordjournals.org/).

Keywords

CDK7 | CDK9 | GBM | GSCs | Self-renewal | xenograft model

Acknowledgments

We thank Dr. Peter Forsyth, Chairman, Neuro-Oncology Program, Moffitt Cancer Center for insightful discussions. Support from the Flow Cytometry Core, Analytic Microsopy Core and other Shared Resources is greatly acknowledged.

Funding

This work was supported by the grant (02-30000-16-10) from the Moffitt Cancer Center (S.P.C.), NIH grant NS115403, NS126810, NS126819, NS122375, and Jean & Lou Malnati Brain Tumor Institute of Northwestern Medicine (S.Y.C.), NIH CA234799 and US AMRAA W81XWH2210373 (D.M.T.). The Shared Resources at the Moffitt Cancer Center is supported by the grant P30-CA076292.

Conflict of Interest statement

The authors declare no conflict of interest.

Authorship statement

IB: conducted experiments, analyzed data and wrote original draft; JP: conceptualized, designed the experiments, conducted experiments, analyzed and interpreted data, and wrote and edited the manuscript; FK: participated in mouse experiments; SKC: provided resource, interpreted the data and edited the manuscript; SYC: provided resource, discussed data and edited the manuscript; DMT: provided recourses; DD: provided resource and edited the manuscript; HL: provided resource and edited the manuscript; MAV: edited the manuscript; QM: helped with TCGA data analysis and edited the manuscript.

Declarations

Ethics approval and consent to participate: NA.

Data Availability

The datasets used and/or analyzed during the current study will be made available upon reasonable request.

Affiliations

Department of Tumor Biology, Moffitt Cancer Center and Research Institute, Tampa, FL, USA (I.B., F.K., S.P.C., J.P.); The Ken and Ruth Devee Department of Neurology, Lou and Jean Malnati Brain Tumor Institute Northwestern Medicine, The Robert H. Lurie Comprehensive Cancer Center, Simpson Querrey Institute for Epigenetics, Northwestern University Feinberg School of Medicine, Chicago, IL, USA (S.-Y.C., D.M.T.); Department of Drug Discovery, Moffitt Cancer Center and Research Institute, Tampa, FL, USA (D.D., H.L.); Department of Neuro-Oncology and Neuro-Oncology Program, Moffitt Cancer Center and Research Institute, Tampa, FL, USA (M.A.V.); Department of Biostatistics and Bioinformatics, Moffitt Cancer Center and Research Institute, Tampa, FL, USA (Q.M.); Department of Molecular Medicine, University of South Florida, Tampa, FL, USA (J.P.)

References

1. Hanif F, Muzaffar K, Perveen K, Malhi SM, Simjee Sh U. Glioblastoma multiforme: A review of its epidemiology and pathogenesis through clinical presentation and treatment. *Asian Pac J Cancer Prev.* 2017;18(1):3–9.
2. Ostrom QT, Cioffi G, Waite K, Kruchko C, Barnholtz-Sloan JS. CBTRUS statistical report: Primary brain and other central nervous system tumors diagnosed in the United States in 2014-2018. *Neuro Oncol.* 2021;23(12 suppl 2):iii1–iii105.
3. Aldape K, Brindle KM, Chesler L, et al. Challenges to curing primary brain tumours. *Nat Rev Clin Oncol.* 2019;16(8):509–520.
4. Stupp R, Mason WP, van den Bent MJ, et al; European Organisation for Research and Treatment of Cancer Brain Tumor and Radiotherapy Groups. Radiotherapy plus concomitant and adjuvant temozolomide for glioblastoma. *N Engl J Med.* 2005;352(10):987–996.
5. Reddy K, Gaspar LE, Kavanagh BD, et al. Prospective evaluation of health-related quality of life in patients with glioblastoma multiforme treated on a phase II trial of hypofractionated IMRT with temozolomide. *J Neurooncol.* 2013;114(1):111–116.
6. Tanzilli A, Pace A, Fabi A, et al. Neurocognitive evaluation in older adult patients affected by glioma. *J Geriatr Oncol.* 2020;11(4):701–708.
7. Cruz Da Silva E, Mercier MC, Etienne-Selloum N, Dontenwill M, Choulier L. A systematic review of glioblastoma-targeted therapies in phases II, III, IV clinical trials. *Cancers.* 2021;13(8):1795.
8. Chow LM, Endersby R, Zhu X, et al. Cooperativity within and among Pten, p53, and Rb pathways induces high-grade astrocytoma in adult brain. *Cancer Cell.* 2011;19(3):305–316.
9. Mai WX, Gosa L, Daniels VW, et al. Cytoplasmic p53 couples oncogene-driven glucose metabolism to apoptosis and is a therapeutic target in glioblastoma. *Nat Med.* 2017;23(11):1342–1351.
10. Todorova PK, Fletcher-Sananikone E, Mukherjee B, et al. Radiation-induced DNA damage cooperates with heterozygosity of TP53 and PTEN to generate high grade gliomas. *Cancer Res.* 2019;79(14):3749–3761.
11. Wang D, Berglund A, Kenchappa RS, et al. BIRC3 is a novel driver of therapeutic resistance in Glioblastoma. *Sci Rep.* 2016;6:21710.
12. Chanez B, Appay R, Guille A, et al. Genomic analysis of paired IDHwt glioblastomas reveals recurrent alterations of MPDZ at relapse after radiotherapy and chemotherapy. *J Neurol Sci.* 2022;436:120207.
13. Clark PA, Iida M, Treisman DM, et al. Activation of multiple ERBB family receptors mediates glioblastoma cancer stem-like cell resistance to EGFR-targeted inhibition. *Neoplasia.* 2012;14(5):420–428.
14. Cruickshanks N, Zhang Y, Hine S, et al. Discovery and therapeutic exploitation of mechanisms of resistance to MET inhibitors in glioblastoma. *Clin Cancer Res.* 2019;25(2):663–673.
15. Jensen KV, Hao X, Aman A, Luchman HA, Weiss S. EGFR blockade in GBM brain tumor stem cells synergizes with JAK2/STAT3 pathway inhibition to abrogate compensatory mechanisms in vitro and in vivo. *Neurooncol Adv.* 2020;2(1):vdaa020.
16. Laks DR, Oses-Prieto JA, Alvarado AG, et al. A molecular cascade modulates MAP1B and confers resistance to mTOR inhibition in human glioblastoma. *Neuro Oncol.* 2018;20(6):764–775.
17. Lathia JD, Mack SC, Mulkearns-Hubert EE, Valentim CL, Rich JN. Cancer stem cells in glioblastoma. *Genes Dev.* 2015;29(12):1203–1217.
18. Jackson M, Hassiotou F, Nowak A. Glioblastoma stem-like cells: At the root of tumor recurrence and a therapeutic target. *Carcinogenesis.* 2015;36(2):177–185.
19. Chen J, McKay RM, Parada LF. Malignant glioma: Lessons from genomics, mouse models, and stem cells. *Cell.* 2012;149(1):36–47.
20. Sharifzad F, Ghavami S, Verdi J, et al. Glioblastoma cancer stem cell biology: Potential theranostic targets. *Drug Resist Updat.* 2019;42:35–45.
21. Badjatia N, Ambrosio DL, Lee JH, Gunzl A. Trypanosome cdc2-related kinase 9 controls spliced leader RNA cap4 methylation and phosphorylation of RNA polymerase II subunit RPB1. *Mol Cell Biol.* 2013;33(10):1965–1975.
22. Padmanabhan J, Brown KR, Padilla A, Shelanski ML. Functional role of RNA polymerase II and P70 S6 kinase in KCl withdrawal-induced cerebellar granule neuron apoptosis. *J Biol Chem.* 2015;290(9):5267–5279.
23. Meng W, Wang J, Wang B, et al. CDK7 inhibition is a novel therapeutic strategy against GBM both in vitro and in vivo. *Cancer Manag Res.* 2018;10:5747–5758.
24. Kwiatkowski N, Zhang T, Rahl PB, et al. Targeting transcription regulation in cancer with a covalent CDK7 inhibitor. *Nature.* 2014;511(7511):616–620.
25. Chen R, Wierda WG, Chubb S, et al. Mechanism of action of SNS-032, a novel cyclin-dependent kinase inhibitor, in chronic lymphocytic leukemia. *Blood.* 2009;113(19):4637–4645.
26. Yin T, Lallena MJ, Kreklau EL, et al. A novel CDK9 inhibitor shows potent antitumor efficacy in preclinical hematologic tumor models. *Mol Cancer Ther.* 2014;13(6):1442–1456.
27. Barlaam B, Casella R, Cidado J, et al. Discovery of AZD4573, a potent and selective inhibitor of CDK9 that enables short duration of target engagement for the treatment of hematological malignancies. *J Med Chem.* 2020;63(24):15564–15590.
28. Cidado J, Boiko S, Proia T, et al. AZD4573 is a highly selective CDK9 inhibitor that suppresses MCL-1 and induces apoptosis in hematologic cancer cells. *Clin Cancer Res.* 2020;26(4):922–934.
29. Olson CM, Jiang B, Erb MA, et al. Pharmacological perturbation of CDK9 using selective CDK9 inhibition or degradation. *Nat Chem Biol.* 2018;14(2):163–170.
30. Wang B, Wu J, Wu Y, et al. Discovery of 4-(((4-(5-chloro-2-(((1s,4s)-4-((2-methoxyethyl)amino)cyclohexyl)amino)pyridin-4-yl)thiazol-2-yl)amino)methyl)tetrahydro-2H-pyran-4-carbonitrile (JSH-150) as a novel

highly selective and potent CDK9 kinase inhibitor. *Eur J Med Chem.* 2018;158:896–916.
31. Rohle D, Popovici-Muller J, Palaskas N, et al. An inhibitor of mutant IDH1 delays growth and promotes differentiation of glioma cells. *Science.* 2013;340(6132):626–630.
32. Song X, Wan X, Huang T, et al. SRSF3-regulated RNA alternative splicing promotes glioblastoma tumorigenicity by affecting multiple cellular processes. *Cancer Res.* 2019;79(20):5288–5301.
33. Giannini C, Sarkaria JN, Saito A, et al. Patient tumor EGFR and PDGFRA gene amplifications retained in an invasive intracranial xenograft model of glioblastoma multiforme. *Neuro Oncol.* 2005;7(2):164–176.
34. Tiek DM, Erdogdu B, Razaghi R, et al. Temozolomide-induced guanine mutations create exploitable vulnerabilities of guanine-rich DNA and RNA regions in drug-resistant gliomas. *Sci Adv.* 2022;8(25):eabn3471.
35. Vaubel RA, Tian S, Remonde D, et al. Genomic and phenotypic characterization of a broad panel of patient-derived xenografts reflects the diversity of glioblastoma. *Clin Cancer Res.* 2020;26(5):1094–1104.
36. Woods N, Trevino J, Coppola D, et al. Fendiline inhibits proliferation and invasion of pancreatic cancer cells by interfering with ADAM10 activation and beta-catenin signaling. *Oncotarget.* 2015;6(34):35931–35948.
37. Woods NK, Padmanabhan J. Inhibition of amyloid precursor protein processing enhances gemcitabine-mediated cytotoxicity in pancreatic cancer cells. *J Biol Chem.* 2013;288(42):30114–30124.
38. Bora-Singhal N, Nguyen J, Schaal C, et al. YAP1 Regulates OCT4 activity and SOX2 expression to facilitate self-renewal and vascular mimicry of stem-like cells. *Stem Cells.* 2015;33(6):1705–1718.
39. Machl A, Wilker EW, Tian H, et al. M2698 is a potent dual-inhibitor of p70S6K and Akt that affects tumor growth in mouse models of cancer and crosses the blood-brain barrier. *Am J Cancer Res.* 2016;6(4):806–818.
40. Ebmeier CC, Erickson B, Allen BL, et al. Human TFIIH kinase CDK7 regulates transcription-associated chromatin modifications. *Cell Rep.* 2017;20(5):1173–1186.
41. Paparidis NF, Durvale MC, Canduri F. The emerging picture of CDK9/P-TEFb: More than 20 years of advances since PITALRE. *Mol Biosyst.* 2017;13(2):246–276.
42. Proud CG. p70 S6 kinase: An enigma with variations. *Trends Biochem Sci.* 1996;21(5):181–185.
43. Fan W, Wang W, Mao X, et al. Elevated levels of p-Mnk1, p-eIF4E and p-p70S6K proteins are associated with tumor recurrence and poor prognosis in astrocytomas. *J Neurooncol.* 2017;131(3):485–493.
44. Zhang H, Pandey S, Travers M, et al. Targeting CDK9 reactivates epigenetically silenced genes in cancer. *Cell.* 2018;175(5):1244–1258.e26.
45. Lacar B, Linker SB, Jaeger BN, et al. Nuclear RNA-seq of single neurons reveals molecular signatures of activation. *Nat Commun.* 2016;7:11022.
46. Sun Z, Xu X, He J, et al. EGR1 recruits TET1 to shape the brain methylome during development and upon neuronal activity. *Nat Commun.* 2019;10(1):3892.
47. Yin L, Banerjee S, Fan J, et al. Epigenetic regulation of neuronal cell specification inferred with single cell "Omics" data. *Comput Struct Biotechnol J.* 2020;18:942–952.
48. Puang SJ, Elanggovan B, Ching T, Sng JCG. MEF2C and HDAC5 regulate Egr1 and Arc genes to increase dendritic spine density and complexity in early enriched environment. *Neuronal Signal.* 2020;4(3):NS20190147.
49. Brito DVC, Kupke J, Gulmez Karaca K, Oliveira AMM. Regulation of neuronal plasticity by the DNA repair associated Gadd45 proteins. *Curr Res Neurobiol.* 2022;3:100031.
50. Chandramouly G. Gadd45 in DNA demethylation and DNA repair. *Adv Exp Med Biol.* 2022;1360:55–67.